

# Creating mock catalogues of stellar haloes from cosmological simulations

Ben Lowing<sup>1\*</sup>, Wenting Wang<sup>1†</sup>, Rachel Kennedy<sup>1</sup>, Andrew Cooper<sup>2</sup>, John Helly<sup>1</sup>, Carlos Frenk<sup>1</sup> and Shaun Cole<sup>1</sup>

<sup>1</sup>*Institute for Computational Cosmology, Department of Physics, University of Durham, South Road, Durham, DH1 3LE, UK*

<sup>2</sup>*National Astronomical Observatories, Chinese Academy of Sciences, 20A Datun Road, Chaoyang, Beijing 10012, P.R. China*

Accepted ... Received ... in original form ...

## ABSTRACT

We present a new technique for creating mock catalogues of the individual stars that make up the accreted component of stellar haloes in cosmological simulations and show how the catalogues can be used to test and interpret observational data. The catalogues are constructed from a combination of methods. A semi-analytic galaxy formation model is used to calculate the star formation history in haloes in an  $N$ -body simulation and dark matter particles are tagged with this stellar mass. The tags are converted into individual stars using a stellar population synthesis model to obtain the number density and evolutionary stage of the stars, together with a phase-space sampling method that distributes the stars while ensuring that the phase-space structure of the original  $N$ -body simulation is maintained. A set of catalogues based on the Aquarius simulations of Milky Way mass haloes have been created and made publicly available on a website. Two example applications are discussed that demonstrate the power and flexibility of the mock catalogues. We show how the rich stellar substructure that survives in the stellar halo precludes a simple measurement of its density profile and demonstrate explicitly how pencil-beam surveys can return almost any value for the slope of the profile. We also show that localized variations in the abundance of particular types of stars, a signature of differences in the composition of stellar populations, allow streams to be easily identified.

**Key words:** methods: numerical, galaxies: haloes

## 1 INTRODUCTION

Large extended diffuse stellar haloes are known to surround both the Milky Way and M31 (Lewis et al. 2013). The  $\Lambda$ CDM model of hierarchical structure formation predicts that these haloes should be a ubiquitous outcome of galaxy formation resulting from the accretion of satellite galaxies that fall into the potential of the larger host galaxy and are subsequently disrupted (Bullock & Johnston 2005; Cooper et al. 2010). The dynamical time of the stellar halo is very long compared to the age of the host galaxy and so they preserve a memory of their initial conditions. From the the identification of distinct populations within haloes, and the study of properties such as kinematics or chemical composition, a vast amount of information about the assembly history of the galaxy can be inferred.

The outer region of stellar haloes is dominated by multiple, extensive tidal streams, while the inner regions, where the dynamical timescales are shorter, experience a more complete destruction of substructure and therefore have a smoother stellar distribution. In addition to the accreted component, stellar haloes are thought to contain a second component made up of stars that formed *in situ*. The exact formation mechanism of the *in situ* component is still uncertain but includes stars scattered out of the galaxy disc at early times (Zolotov et al. 2010; Font et al. 2011a). The *in situ* component dominates in the inner few kiloparsecs and could be important out to  $\sim 30$ kpc. This view is supported by recent observations of the Milky Way, (Carollo et al. 2007, 2010), which have suggested that the stellar halo contains at least two distinct components.

Over the last few years there has been much effort dedicated to modelling stellar haloes (Bullock & Johnston 2005; Cooper et al. 2010; Zolotov et al. 2010; Font et al. 2011a; Tissera et al. 2012) motivated by improvement in observations.

\* E-mail: b.j.lowing@durham.ac.uk

† E-mail: bilinxing.wenting@gmail.com

Recent surveys such as SDSS (York et al. 2000) and Pan-STARRS (Kaiser et al. 2010) have started to probe deeper into the Milky Way halo and are starting to build up a picture of its complex structure. The forthcoming GAIA mission (Prusti 2012) will lead to further major improvements (Jordi et al. 2010; de Bruijne 2012). We are now at the point where careful comparisons between the haloes predicted by theory and those observed in the universe are becoming possible.

In order to make a direct comparison of theoretical predictions with observations of stellar haloes, a model of stellar halo formation is required, along with a way to convert the output into observable quantities. Many simulations of stellar haloes have been carried out (Bullock & Johnston 2005; Zolotov et al. 2010; Tissera et al. 2012), but usually for isolated galaxies. To obtain realistic accretion histories, a complete model of galaxy formation in a cosmological context is essential. Current cosmological hydrodynamical simulations do not yet have sufficient power to resolve the detailed structure within stellar haloes but can provide information about their general properties (e.g. Crain et al. 2009; Vogelsberger et al. 2014). Since only a small fraction of the stellar mass of a galaxy is in the halo, even “zoom” simulations of individual galaxies, still contain a relatively low number of halo star particles.

In this paper we employ the particle tagging method developed by Cooper et al. (2010, hereafter C10) to construct stellar halo models. The method is based on high-resolution dark matter simulations in which the star formation occurring in haloes is calculated using a semi-analytic galaxy formation model. At every output time in the simulation, an appropriate set of dark matter particles is tagged with the stellar mass that formed since the previous output time. The advantages of this technique are that it can create models of much higher resolution and at a much lower computational cost than full hydrodynamical simulations. C10 demonstrated that the method produces complex stellar haloes containing tidal streams, shells and other substructure, whose ages and metallicities are in broad agreement with recent observations.

A limitation of the C10 tagging method is that “star particles” are not individual stars but rather represent entire stellar populations which can contain thousands of solar masses of stars. The challenge is to compare these sparsely populated haloes to actual observational surveys which often focus on a particular type of star, such as blue horizontal branch (BHB) stars. These may not trace the overall stellar mass distribution in an unbiased way. To overcome this limitation, we use a method similar to that employed in GALAXIA (Sharma et al. 2011) to construct customizable mock catalogues of halo stars. Each star particle is treated as a separate simple stellar population using theoretical isochrones to determine the abundance of each type of star expected in a population of that age and metallicity. To create positions and velocities of individual stars, the star particle distribution is oversampled using a phase-space method based on the EnBiD code (Sharma & Steinmetz 2006) which maintains the underlying phase-space structure.

Our mock catalogues allow us to compare the actual structure of the stellar haloes constructed from the simulations to that measured observationally. Obscuration by the Milky Way disc, limited survey regions and a small number of tracers mean that the structure of the stellar halo of our

Galaxy is only sampled in small patches of the sky. Nevertheless, attempts are often made to infer the shape and profile of the Milky Way stellar halo from these limited observations (e.g. Helmi 2008; Deason et al. 2013). In this paper we show how the complicated uneven structure of the outer accreted stellar halo renders global properties unmeasurable by any sort of local observations. In addition, the mock catalogues allow us to identify features in stellar haloes that may potentially leave signatures that can be searched for in observations. For example, we show how differences in the satellites that build up the stellar halo result in variations in the composition of different stellar populations and thus in local variations in the ratio of stellar types. This approach can potentially help to detect new streams in the Milky Way.

In Section 2 we outline the methods used to create stellar halo models. The final output of the process, a set of mock catalogues of individual stars and their properties, is described in further detail in Section 3. Sections 4 and 5 present two simple example applications of the mock catalogues to study the overall structure of stellar haloes in our simulations and the distribution of different stellar types over the sky. Finally, in Section 6 we discuss some potential advanced applications of the mock catalogues and how they can be used to interpret and test observational strategies.

## 2 METHOD

Creating a model of stellar haloes based on a consistent theory of galaxy formation in a cosmological context requires a combination of various techniques. The foundation of our models is a set of  $N$ -body dark matter only “zoom” simulations of Milky Way mass haloes onto which we have grafted the Durham semi-analytic model of galaxy formation, GALFORM (Cole et al. 2000). GALFORM predicts the amount of stars that form in every halo and subhalo at each output time, along with an estimate of the metallicity of each stellar population. This stellar mass is then assigned to dark particles within the  $N$ -body simulations using the C10 particle tagging technique, which allows us to track the accretion and disruption of satellites and follow the fate of the stripped stellar material. Finally, to convert the massive simulation particles into mock catalogues we use a method based on stellar population modelling and phase-space sampling. Each of these steps is briefly outlined in the following subsections.

### 2.1 $N$ -body Simulations

For this work we use the haloes from the Aquarius project of simulations, which involves six dark matter haloes of mass  $\sim 10^{12} M_{\odot}$  at multiple resolutions (Springel et al. 2008a,b; Navarro et al. 2010). The simulations assume the standard  $\Lambda$ CDM cosmology with parameters chosen to be consistent with the results from the *WMAP* 1-year data (Spergel et al. 2003) and the 2dF Galaxy Redshift Survey data (Colless et al. 2001): matter density parameter,  $\Omega_M = 0.25$ ; cosmological constant,  $\Omega_{\Lambda} = 0.75$ ; power spectrum normalization,  $\sigma_8 = 0.9$ ; spectral index,  $n_s = 1$ ; and Hubble parameter  $h = 0.73$ . The six haloes were selected randomly from a set of isolated  $\sim 10^{12} M_{\odot}$  haloes identified in a lower resolution ( $900^3$ -particle) parent simulation of a  $100h^{-1}$  Mpc

cubic volume (Gao et al. 2008). The isolation criterion requires a halo to have no neighbours exceeding half its mass within  $1h^{-1}$  Mpc. This is a weak selection criterion that ensures that the haloes are not members of any massive groups or clusters.

We have used only five of the six Aquarius haloes, since the last of them underwent two major mergers at late times  $z \sim 0.6$  making it unlikely to be the host of a disc galaxy at  $z = 0$ . We use the standard Aquarius naming convention using the abbreviations Aq-A to Aq-E to refer to the five haloes; in each case we use the second highest resolution (“level-2” in the Aquarius notation) simulation, with a particle mass of at most  $10^4 h^{-1} M_{\odot}$ . For each of the Aquarius simulations we have used 128 outputs, corresponding approximately to one output every 155 Myr at late times.

## 2.2 Galaxy Formation Model

Dark matter  $N$ -body simulations are ideal for following the large-scale and non-linear growth of cosmic structure, including the detailed accretion history of a halo. Of course they follow only the dark matter component. Including the baryonic component in a realistic manner at sufficient resolution in a cosmological simulation is still computationally prohibitive. Fortunately, semi-analytic galaxy formation models do not suffer from these limitations and are ideal for our purposes. Based on simple theoretical treatments and empirical prescriptions, these models provide a good match to a remarkable number of observations of the local and distant galaxy populations (Baugh 2006). These models, however, are not designed to follow the internal structure of galaxies in detail.

The Durham semi-analytic model, GALFORM, is used in this work to postprocess the Aquarius  $N$ -body simulations and calculate the star formation occurring in each subhalo. This provides the mass of stellar material that formed between two simulation outputs, along with its metallicity. Rather than using the Bower et al. (2006) model on which C10 was based, we use the more recent Font et al. (2011b) model, which includes a modified treatment of physics relevant to satellites. The Font et al. (2011b) model produces a satellite luminosity function that matches that of Milky Way and also generates stellar populations in satellites which have the correct metallicities required to match the observed luminosity-metallicity relation. The main changes compared to the Bower et al. (2006) model are the use of a higher yield, a saturated feedback model for supernovae, in which the feedback efficiency saturates in small-mass haloes, with  $v_{\text{circ}} \leq 65 \text{ km s}^{-1}$ , and earlier reionization. This new GALFORM model eliminates a shortcoming of C10 where the overall metallicity of the stellar halo was found to be significantly lower than that of the Milky Way.

## 2.3 Particle Tagging

The C10 particle tagging method is a means to associate the stellar mass calculated by GALFORM with spatial locations in haloes identified in high-resolution dark matter only simulations. After applying GALFORM to the outputs of the Aquarius simulations C10 tagged the predicted stellar mass onto the 1% most bound dark matter particles in the corresponding haloes at the appropriate times. These tagged

dark matter particles can be located in the final snapshot to track where the stellar mass ended up. This method is ideal to study the formation of the outer accreted component of stellar haloes but a potential disadvantage is that the stellar material is restricted to following the dynamics of a subset of the dark matter, ignoring any potential effects of baryons on the structure of the haloes (see e.g. Sawala et al. 2013). However, for dark matter dominated objects such as satellites, these effects are expected to be unimportant.

## 2.4 Mock Catalogue Construction

The final step is to turn the output of the tagged simulations into full mock catalogues of individual stars. The output of the model is a collection of particles, each tagged with some amount of stellar mass, and having both an age for when the stars were born and a metallicity at that time. When a single dark matter particle has been tagged multiple times, we treat it as separate tagged particles occupying the same position. Turning this into a full mock requires two steps. The first is to determine the number of stars of different types that each tagged particle represents by considering each one as a simple stellar population, and the second step is to distribute these stars over an appropriate phase-space volume in order to increase the sampling and create individual stars. The following subsections discuss each step in detail.

### 2.4.1 Stellar Population Synthesis

Unfortunately, even with the high-resolution Aquarius simulations we are a long way from being able to represent individual stars by single particles. Instead, each stellar particle can represent up to thousands of solar masses. In order to convert the massive stellar particles into individual stars we consider each tagged particle as a single stellar population (SSP), in which all the stars formed at the same time from gas with the same metallicity; the theoretical justification of this is discussed in detail in Pasetto et al. (2012). The abundances of the different star types that make up the population can then be obtained using stellar population synthesis modelling.

A chosen initial mass function (IMF) determines the number of stars forming within each stellar population as a function of initial stellar mass. Here we adopt a Kennicutt IMF with no correction for brown dwarfs (Kennicutt 1983), just as was used in the semi-analytical model to ensure consistency. Theoretical stellar isochrones then specify whether each type of star still survives at the final time, along with the current properties of these stars.

The stellar isochrones allow us to assign properties such as temperature, magnitude and colour to stars of a given initial mass, age and metallicity. We employ the PARSEC isochrones (Bressan et al. 2012), as these are recent, up-to-date isochrones that extend over a wide range of metallicities ( $0.0001 \leq Z \leq 0.06$ ). We create a grid of isochrones spanning the range of ages between  $6.63 < \log_{10} t/\text{yr} < 10.13$ , with a step size ( $\Delta \log(t) = 0.0125$ ), and a range of metallicities between  $0.0001 \leq Z \leq 0.005$ . Interpolating between ages and metallicities would require matching different evolutionary points along the isochrones, so instead we simply identify the nearest isochrone in the grid and associate that

with a tag. A finer grid could be used if required, but the adopted resolution was found to be adequate for our current purposes.

The method can be summarized as follows: for each tag, split the population into a range of initial stellar mass bins. Use the IMF to determine the fractional weighting of each bin. Then find the closest isochrone in age and metallicity and use that to assign properties to the stars in each bin. Finally, multiply the mass of the tag by the weight of the bin to obtain the total mass and, from that, the number of stars in that bin. Not all the mass of the tag will be converted into stars: high mass stars that evolved rapidly and no longer survive will be absent from the final population, even though they may have accounted for a large fraction of the tag mass.

#### 2.4.2 Phase space Sampling

The next step is to split the massive stellar particles representing SSPs into single stars with individual positions and velocities. While the massive stellar particles provide a coarse sampling of the phase-space distribution of the stellar halo, it is desirable to smooth the distribution and increase the sampling. This is done by distributing the mass over the entire phase-space volume that the particle represents. Using the phase-space volume rather than just the real-space volume allows coherent structures such as streams to be maintained. It must be noted that increasing the sampling does not increase the resolution and cannot reveal any more detailed structure than was in the original simulation.

To estimate the phase-space volume each stellar mass particle occupies we have used the entropy-based binary decomposition (EnBiD) code of Sharma & Steinmetz (2006). EnBiD numerically estimates the densities of discretely sampled data based on a binary space partitioning tree. EnBiD uses an entropy-based node splitting criterion to decide which subspace (real or velocity space) to split next. This makes the method metric free, as there is no need to specify in advance how velocity and configuration spaces relate to each other, and ensures the subspace with greater variation is subdivided more.

Once the binary tree has been built, the leaf nodes can be used to estimate the phase-space volume of each particle. The volume of the hypercube of the leaf nodes can vary significantly even between close neighbours due to Poisson sampling noise of the original particle distribution. Simply using the volumes of raw nodes would result in a large dispersion, but this can be reduced by using a smoothing scheme. We have modified EnBiD's anisotropic kernel density estimation scheme to return a volume as well as a density. The scheme works by first calculating a local metric about each particle based on the shape of the hypercube of each leaf node and using the length of the six sides to scale the phase space in each direction. A covariance matrix is then calculated based on the nearest 64 neighbours in the scaled space. Diagonalizing the covariance matrix gives a set of eigenvalues and eigenvectors that can be used to perform a further transformation to a coordinate system in which the eigenvectors define the principal axes. In this new rotated and scaled space the local particle distribution will have unit covariance in each direction. Finally, the phase-space volume of the particle is defined as a hypersphere with 1/40 of the volume of a hypersphere based on the distance to the 40th

nearest neighbour,  $R_{40}$ . It therefore has a radius  $R_1$  of

$$R_1 = \left(\frac{1}{40}\right)^{1/6} R_{40}. \quad (1)$$

The modified version of EnBiD returns a 6x6 matrix that describes the phase-space volume of each particle.

The actual sampling is performed by choosing points from an 6d isotropic Gaussian distribution in which each component has zero mean and variance  $\sigma^2 = \gamma R_1^2$ . Each generated point is then transformed by applying the inverse operations to convert from the sampled space back to positions and velocities in the original simulation. Some care has to be taken with the choice of the scale parameter  $\gamma$  which relates the scale of the Gaussian kernel to the scale of the hypersphere returned by EnBiD. Choosing too large a value of  $\gamma$  will result in the phase space structure of each component of the halo being made hotter and too diffuse. Choosing too small a value of  $\gamma$  will result in an artificially clumpy phase space distribution. As a compromise we have chosen  $\gamma = 1/48$ . In a separate study (Wang et al in preparation) we have developed a maximum likelihood method for modelling the distribution function of the stellar halo in order to estimate the mass of the host dark matter halo. Using this approach we have found that the recovered halo mass is biased high if  $\gamma$  is too large. With  $\gamma = 1/48$  the level of the bias is controlled to be less than about 10%, which is much smaller than typical measurement errors. Much smaller values of  $\gamma$  would remove this bias entirely, but would negate the benefit of the phase sampling as in the limit  $\gamma \rightarrow 0$  one is merely placing all the stars at the same phase-space location as the tagged particle from which they arise.

In order to test our EnBiD sampling method and demonstrate that we have made a suitable choice for the parameter  $\gamma$  we look at how well it performs at resampling a down-sampled test satellite. We extracted from the simulation a satellite, containing 15,250 particles, that is in the process of undergoing significant tidal stripping, so is extended in both real and velocity space. A lower resolution version was created by randomly selecting 10 percent of the particles. Finally, the low resolution version was then resampled using the EnBiD method, with each particle being converted back into 10 particles, thus creating an object with the same resolution as the original extracted test satellite. A comparison between the two then demonstrates the success of our phase space sampling method.

Fig. 1 shows various projections of the different versions of the satellite. The top row is a real-space projection and the bottom row a velocity projection. The original satellite (left column) has a large amount of structure in both real and velocity space, with several complete wraps of the tidal tails visible. In the down-sampled version (middle column) the primary features are still present but the subtle ones are missing, while the non-disrupted remnant of the satellite is more prominent. The EnBiD up-sampled version (right column) is remarkably similar to the original satellite, though the subtle features tend to be smoothed out. In particular the large arc in velocity space at  $v_\theta \approx 400 \text{ km s}^{-1}$ , while still present, is less well resolved. This is expected, as the information about the satellite structure is lost during the down-sampling and no sampling scheme, no matter how complicated, will be able to recover it.

A further test of how well the original and EnBiD ver-

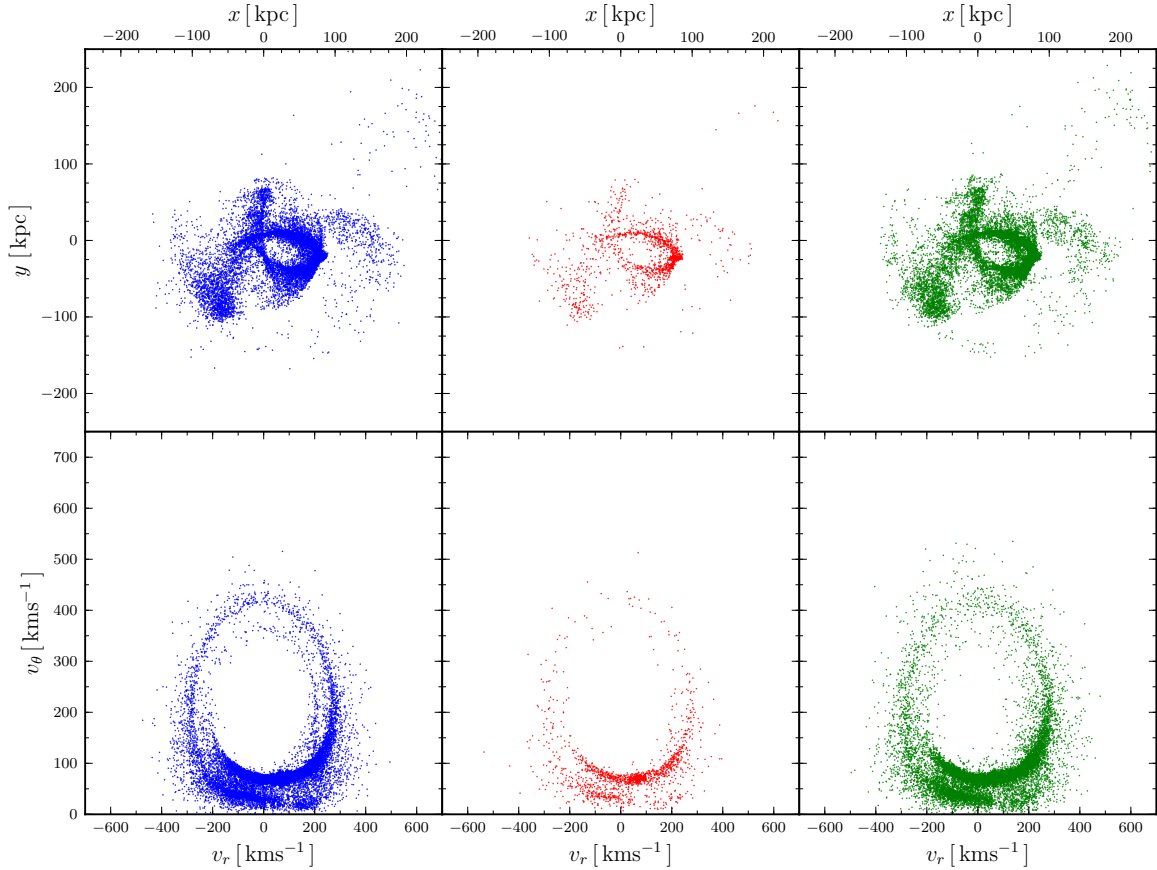


**Figure 1.** Real-space projection of a test satellite (upper row) and velocity-space projection (bottom row). The left column shows the original extracted satellite, while the middle column is the down-sampled version with just 10 percent of the number of particles. Finally, the right column shows the EnBiD version which has been resampled back up to the original resolution.

sions match is a comparison between the volume distribution function of phase-space density,  $v(f)$ , as can be seen in Fig. 2. The technique of Arad et al. (2004), based on Delaunay tessellation, has been used as an independent measurement of the phase-space density. The same volume distribution function is found for all three cases, suggesting that it is robustly defined by even a small subset of the particles and that the EnBiD resampling process does not alter it.

We also notice that at the low density end of Fig. 2 the red dashed curve based on the down-sampled particles starts to plunge at  $f \sim 10^{-14.5}$ , whereas the blue curve based on the original sample continues to increase down to  $f \sim 10^{-15.5}$ . The down-sampled particles are more sparsely distributed in phase space and thus sample poorly low density regions as well as having larger Poisson noise. The green dot-dash curve, which is based on the particles resampled with EnBiD, recovers the same small scale behaviour of the original particle distribution.

When applying the sampling technique to the tagged particles an important consideration is how the particles are divided into subsets on which to run EnBiD. The particular subset that is chosen defines which particles will be considered as phase-space neighbours. We choose to apply the EnBiD sampling to all the tagged particles that form within

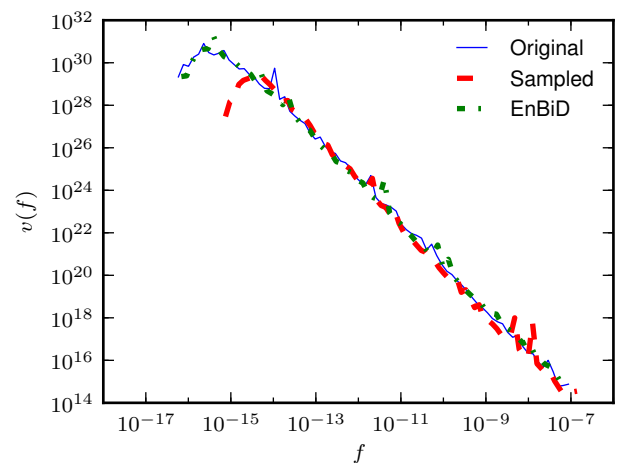


**Figure 2.** Comparison of the volume distribution function of phase-space density,  $v(f)$ , for the different versions of the test satellite. Both axes have arbitrary units.

the same branch of a subhalo merger tree. This separates

the tagged particles into sets based upon the subhalo they formed in.

It is also possible to split the tagged particles by individual assignments. In other words, whenever star formation occurs in a halo and stellar mass is assigned to a set of dark matter particles, just those particles in that assignment are regarded as phase-space neighbours, resulting in a subset of tags with uniform age and metallicity. This has the advantage that the phase-space volumes are not diluted by stars forming later. However, the problem with this method is that the sets of particles in individual assignments are often so small that their phase-space volumes are very large due to an insufficient number of particles to constrain the structure in 6d. While our implementation allows either method to be used, we have chosen to use the first method in the rest of this paper.

EnBiD requires a minimum of 64 particles for the covariance matrix calculation. We therefore exclude assignments with smaller numbers of particles than this. We have checked that this eliminates a negligible amount of stellar mass.

#### 2.4.3 Errors and Extinction

Through the combination of the stellar population synthesis modelling and the phase-space sampling, a mock catalogue of individual stars can be created. However, all the resulting stars will have perfect observational quantities as determined from the models. In order to make the catalogue more realistic and allow direct comparison with survey data, additional uncertainties can be added into the various stellar properties. The exact nature of the errors depends on the detail of the survey that the mock is trying to emulate.

Similarly, stellar observations usually suffer from extinction and this may need to be taken into account. Various models can be applied; however, for observations of the stellar halo away from the Milky Way disc, extinction is not important and thus we have not included its effects in our initial mocks.

## 3 MOCKS

In this section we describe in more detail the range of information that is contained within our mock catalogues, and present a set of example mocks generated from the Aquarius simulations. The combination of the various techniques used results in a rich dataset. The dark matter  $N$ -body simulations used as the foundation of the mocks contain both detailed spatial and detailed kinematical information. Each generated star is associated with a dark matter particle, so its entire history can be traced back through the simulation. The satellite which brought the star into the main halo can be identified, along with the time of accretion of that satellite and the time at which the particle was stripped from the satellite. In addition to the properties of individual stars, by looking at groups of stars, such as all those that originated in the same satellite, it is possible to find candidate stellar structures and streams easily.

The semi-analytical galaxy formation model GALFORM uses physically-motivated prescriptions to follow the evolution of the galaxies within each halo. While GALFORM out-

puts many properties for each galaxy, it is only the star formation and chemical history that are utilized in building the mocks. Nevertheless, these two model predictions for the baryonic components of satellites are essential quantities required to populate the halo with stars. The final input are the theoretical isochrones that provide the detailed properties of the stars. For a given age and metallicity, together with an IMF, the isochrones provide a breakdown of observable stellar properties.

Often when using mock catalogues it is desirable to place the observer within the catalogue itself so as to view the stars in a similar manner to our view of the Milky Way. In order to do this we need first to define a plane that a galactic disc would likely lie in and then choose a position within that plane. We choose to orient the disc plane perpendicular to the semi-minor axis of the moment of inertia of the dark matter in the inner 10 kpc, as the semi-minor axis is a stable orbital axis. While the inclusion of baryons might be expected to change the shape of the centre of the halo due to adiabatic contraction (Kazantzidis et al. 2004), their presence is unlikely to alter the halo's orientation. We have taken the Sun to be 8 kpc from the centre of the galaxy and moving with a velocity  $(U, V, W)_{\odot} = (11, 232, 7) \text{ km s}^{-1}$  (Schönrich et al. 2010). The observer has been placed on the  $x$ -axis, though any orientation on the solar circle would be an equally valid choice.

### 3.1 Example Mocks

We now describe a set of example mock catalogues generated from the Aquarius simulations and use them to illustrate how particular samples of stars can be easily selected. Each sample is defined by a set of colour and magnitude cuts that selects a particular stellar type commonly used for surveying the stellar halo. The overall colour-magnitude diagram for all the stars in the stellar halo of Aq-A (with the contribution from stars still bound in satellites removed) is shown in Fig. 3. The selections for our three samples of halo tracers are marked by boxes.

The vast majority of stars are low mass stars that have never evolved off the main sequence and contain a significant fraction of the total stellar mass. However, these are very faint and, as such, can only be observed in the local stellar neighbourhood and are of little interest when studying the halo. A clear red giant branch and horizontal branch are visible; these contain the older, brighter stars that can be seen to a greater depth, and thus are most useful when studying the structure of the halo.

For these idealized mocks we have not added any additional sources of contamination, or assigned any errors to the observed quantities. Both sources of error can be easily added into the catalogues. The first requires a contamination model describing the distribution of disc stars or extragalactic sources, while the second depends on the survey specifications and limits.

#### 3.1.1 MSTO

Main sequence turn off (MSTO) stars can be unambiguously selected using the colour cut  $0.2 < g - r < 0.4$ , from Bell et al. (2010), and an absolute magnitude cut  $M_g > 4$ , in

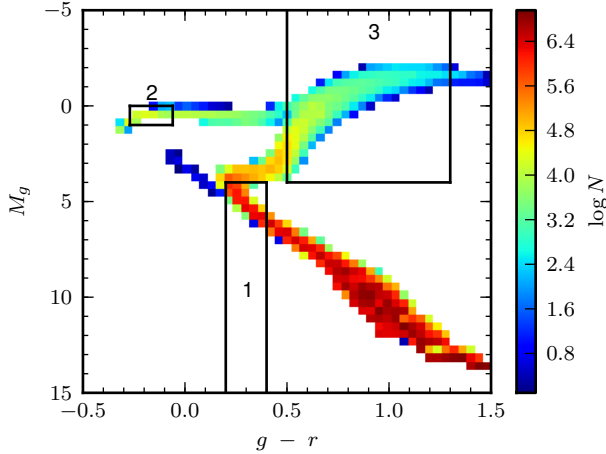


**Figure 3.** Colour-magnitude diagram for the overall stellar population of the accreted stellar halo of Aq-A. Stars still bound to satellites are not included. The colours encode the number of stars within a bin and the boxes show our three mock catalogue selections. Box 1 marks the colour and magnitude cuts used to select MSTO stars, box 2 marks the selection for BHB stars and box 3 the selection for K giants.

order to only select dwarf stars and remove giants. MSTO stars are reaching the end of hydrogen fusion in their core and are about to move to the red giant branch. They are very numerous and therefore serve as a good proxy for the general stellar content of the stellar halo. Approximately 40% to 50% of the total mass embedded in stars brighter than  $M_g = 7$  is found in MSTO stars and there are 81,510,020 such stars in the Aq-A halo. The main reason they are not often used for studying the stellar halo is that they are several magnitudes fainter than the other tracers.

### 3.1.2 BHB

Blue horizontal branch (BHB) stars are a very popular tracer of the stellar halo. They are luminous and have a very nearly constant magnitude,  $M_g \sim 0.7$ , so can be seen to large distances that can be determined accurately from photometry alone. The conditions under which they form are still not well understood, which makes the exact abundance in a mock catalogue sensitive to how they are treated by the theoretical isochrones.

BHB stars can be selected in colour space using the following criteria:  $0.98 < u-g < 1.28$ ,  $-0.27 < g-r < -0.06$  and  $([u-g-0.98]/0.215)^2 + ([g-r+0.06]/0.17)^2 < 1$  (Bell et al. 2010). The main problem in observational selections is that BHB samples are usually heavily contaminated by fainter blue straggler stars. The formation of blue stragglers is also not fully understood, but is thought to be related to binaries. They are not included in the PARSEC isochrones, so are not a source of contamination in the mocks. The number of BHB stars makes up a small fraction of the total mass in stars brighter than  $M_g = 7$ , ranging from 1-3% in the five mocks, with as few as only 242,366 BHBs in the Aq-A halo.

### 3.1.3 K giants

K giants are another stellar type frequently used to map the Milky Way’s stellar halo (Morrison et al. 1990, 2000; Starkenburg et al. 2009). They have the advantage that they are found in predictable numbers in old populations of all metallicities. However, unlike other standard candles, their luminosities range by two orders of magnitude, which makes obtaining accurate distances more challenging. K giants are one of the types that have been targeted for spectroscopy by the Sloan Extension for Galactic Understanding and Exploration (Yanny et al. 2009, SEGUE) and recently, Xue et al. (2012) have estimated distances to a sample of 4781 K giants using a combination of observed  $g-r$  colours and spectroscopic metallicity.

In order to isolate K giants in our stellar halo models we have used the colour cuts  $0.5 < g-r < 1.3$  and  $0.5 < u-g < 3.5$  from Xue et al. (2012), along with their proposed empirical polynomial relation between  $(g-r)$  and  $[\text{Fe}/\text{H}]$  to remove red horizontal branch and red-clump (RC) giants. Anything with  $(g-r) > 0.086 [\text{Fe}/\text{H}]^2 + 0.38 [\text{Fe}/\text{H}] + 0.96$  is excluded from the selection. An additional cut of  $M_g < 4$  removes faint dwarf stars of the same colours. Our selection results in the subset of stars contained within box 3 of Fig. 3, with a large fraction of the stars at the fainter end removed as being either red horizontal branch or red-clump giants. About 6–7% of the total stellar halo mass in stars brighter than  $M_g = 7$  is found as K giants and there are 881,507 K giants in the Aq-A halo.

## 3.2 Public Catalogues

These five complete mock catalogues for the Aquarius haloes A-E will be made publicly available at the following website <http://virgodb.dur.ac.uk:8080/MyMillennium>. They contain all stars with  $M_g < 7$ . Each mock is stored in a separate table within the StellarHalo database and can be accessed via the web interface using SQL queries. Table 1 lists the information that is provided. Positions, velocities and magnitudes are given relative to both the centre of the halo and to an observer placed in a position similar to that of the Sun. Magnitudes are included for the SDSS  $u, g, r, i, z$  filters.

## 3.3 Limitations

While the mock catalogues we have generated are based on sophisticated cosmological models, they are not without certain limitations. The biggest limitation is that our model only generates the accreted component of the stellar halo. The *in situ* component that dominates in the inner region, along with any kind of galactic disc, are missing. This means that the model is most suitable for studying the outer regions of a galaxy ( $r > 20$  kpc). There are various possible ways to add in additional components to create a more complete model of the entire galaxy, and we will explore these in future papers.

Not only are the stars belonging to the galactic disc excluded from the mock, but the effect of having a disc present within the halo during its evolutionary history is also missing. Subhaloes that pass near or through a disc are more likely to be disrupted and have a shorter lifetime (D’Onghia

Field	Data type	Unit	Description
ID	long		ID of the star, unique within the mock catalogue
Position ( $x, y, z$ )	float	kpc	Star position, relative to halo centre
Velocity ( $v_x, v_y, v_z$ )	float	km s <sup>-1</sup>	Stars velocity, relative to halo rest frame
Galactic coordinates ( $l, b$ )	float	°	Galactic longitude and latitude relative to solar observer
Radial distance ( $r$ )	float	kpc	Distance from solar observer
Relative velocity ( $v_r, v_\theta$ )	float	km s <sup>-1</sup>	Radial and tangential velocity relative to solar observer
Age	float	Gyr	Age of star
Metallicity	float		Fraction of star mass in metals
Mass	float	$M_\odot$	Current mass of star
$\log_{10}(g)$	float	log(cgs)	Surface gravity of the star
$\log_{10}(T_{eff})$	float	$\log_{10}(K)$	Effective temperature of the star
Type	int		The type of star based on its currently evolutionary stage
$M_{(u,g,r,i,z)}$	float		Absolute rest frame ( $u,g,r,i,z$ ) band (SDSS) magnitude of the star
$m_{(u,g,r,i,z)}$	float		Apparent rest frame ( $u,g,r,i,z$ ) band (SDSS) magnitude of the star as seen by the solar observer
Dark Matter ID	long		The tagged dark matter particle this star was spawned from
Subhalo ID	long		The current subhalo to which the associated dark matter particle belongs to. -1 if not currently a member of any subhalo, 0 if part of the main halo
Tree ID	long		The subhalo tree that this star came from. All stars that arrive in the main halo via the same satellite have the same ID
Infall Redshift	float		Accretion redshift of the subhalo this star once belonged to

**Table 1.** Information provided in our online mock catalogues that may be accessed at <http://virgodb.dur.ac.uk:8080/MyMillennium>. SQL can be used to query any of these fields.

et al. 2010). The importance of such effects is unclear because the disk has been growing as the halo grows and, even today, it presents a small cross section to infalling satellites. Thus, any effects of this sort will, if at all, only affect satellites that pass close to the centre of the halo and not the recent ones that are falling into the halo for the first time.

The C10 technique relies on tagging the most bound dark matter particles in a subhalo. This means that the stars are constrained to have the same distribution and dynamics as the tagged dark matter particles. In reality stars form may satellites with significantly different configurations and dynamics, such as in flattened disc structures. For this reason, the spatial configuration of stars within satellites is likely to be unreliable; however, once the satellite has been disrupted and the stars stripped, the importance of their initial configuration is diminished.

#### 4 DENSITY PROFILE OF THE STELLAR HALO

One of the most basic, but still unanswered, questions in galactic structure is the shape and profile of the Milky Way stellar halo. While there is now general consensus that the stellar halo is oblate and follows a broken power-law density profile, the exact form is still ill constrained. RR Lyrae (RRL) variable stars have been commonly used as a tracer, as they are bright standard candles that can be seen to large distances, and are metal poor and very old, so should reflect the distribution of the halo. In addition, they are relatively common and easy to recognize. Keller et al. (2008) and Akhter et al. (2012) found that the spatial density distribution of RRLs in the halo has a power-law slope that significantly steepens at a break radius around  $\sim 45$  kpc. A similar profile was found by Watkins et al. (2009) and

Sesar et al. (2010), who used a sample of RRLs from SDSS Stripe 82, but they measured the break to be located at slightly smaller distances of 25 kpc and 30 kpc respectively.

Measurements using other types of tracers have also suggested the existence of a break in the density profile of the Milky Way. Deason et al. (2011), using a large sample of BHB and blue straggler stars from SDSS DR-8, again found the profile to follow a broken power law, with a break radius at  $\sim 27$  kpc. Similarly, from a sample of near main-sequence turn off (MSTO) stars from the Canada-France-Hawaii Telescope Legacy Survey (CFHTLS), Sesar et al. (2011) measured the break to be at  $\sim 28$  kpc. In contrast, no break or slope steepening was seen by De Propris et al. (2010), who analyzed a sample of 666 BHB stars in two different directions separated by about  $150^\circ$  on the sky. Instead they found a smooth stellar distribution obeying a single power-law density profile of index  $\sim -2.5$ . Akhter et al. (2012) suggested that an explanation for these differences in the measured location of the break could be that at larger distances the outer halo is not be smooth but dominated by clumps and debris.

In Fig. 4 we show the density profiles of the accreted stellar haloes in our five simulations. Three of them show clear breaks, although generally at larger distances than estimated for the Milky Way. To check whether the type of tracer makes a difference we also show in Fig 5 the stellar density profile of the Aquarius A halo measured from different types of tracer stars similar to those used in the observational studies. The overall density profile is that of all stellar material in the tags from the C10 method, while the tracer profiles are from samples taken from the example mock catalogue described in Section 3.1. All of the curves have the same shape, with the break occurring at the same radius, but with differing normalizations, depending on the abundance of the stellar type.

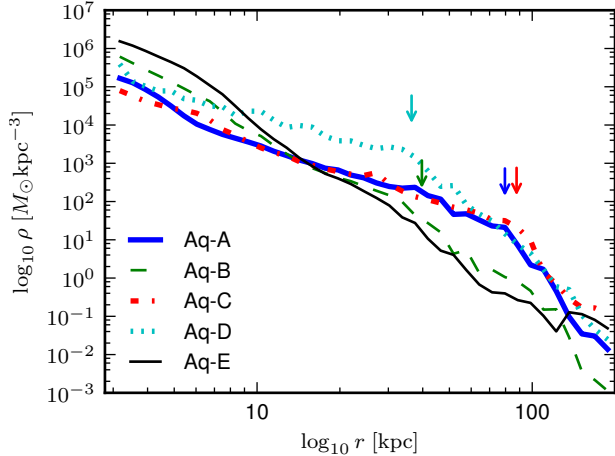


**Figure 4.** The spherically averaged density profiles of the five Aquarius stellar haloes. The arrows show the location of the break in a best-fit broken power law. Three out of the five haloes have clear breaks, a fourth has a weak break while the other one is well fitted by a single power law.

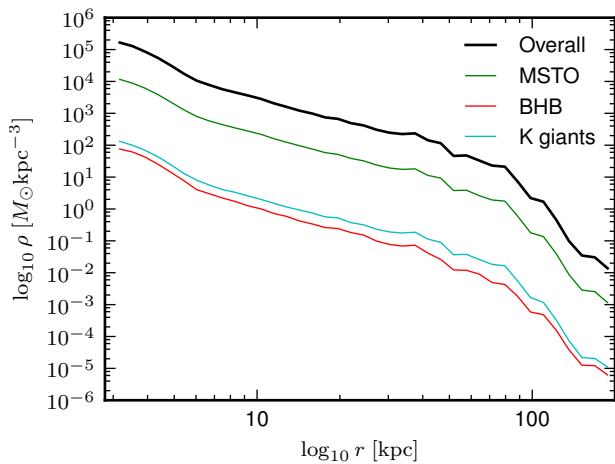


**Figure 5.** The spherically averaged density profile of the Aq-A stellar halo obtained using different types of tracer stars as indicated in the legend. The black line shows the density profile of all stellar material in the halo.

It has been suggested that the presence of a break in the Milky Way’s density profile occurs at the transition between an inner region where the halo is dominated by in-situ stars and an outer region which is primarily composed of accreted halo stars. However, this explanation cannot be correct for the breaks seen in the profiles of the mock catalogues, since they do not contain any in-situ component. More recently, Deason et al. (2013) have proposed that the breaks in stellar halo profiles are related to the recent satellite accretion history of a galaxy. Satellites that are just falling into the halo and are still in the process of being tidally disrupted, may have already lost a significant fraction of their stars by tidal stripping. While these stripped stars are unbound and now form part of the halo, this tidal debris is still in the form of large coherent structures on similar orbits as their progenitor satellites. The merit of measuring a density profile

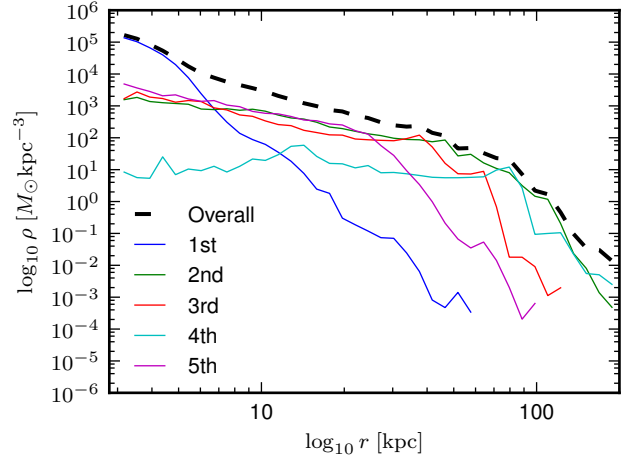


**Figure 6.** The density profile of the Aq-A stellar halo broken down into the five satellites which each contribute the largest amount of mass to the stellar halo.

for such objects is questionable, as they are far from being spherical, but if a spherically averaged profile is constructed for them then they generate flat profiles with very sharp breaks.

In Fig. 6 we show the density profiles of the material that was brought in by the five largest contributors to the Aquarius A stellar halo. Except for the very largest contributor, the profiles of the others all have very strong breaks. A visual inspection reveals that the largest contributor was accreted earliest and, by the end of the simulation, it has been completely disrupted and mixed, with a correspondingly smooth profile. In contrast, the 4th largest contributor has fallen in more recently and is still in the form of a coherent, massive stream. It has a completely flat inner profile and a sharp break around  $\sim 80$  kpc. The other three contributors are in intermediate stages of disruption but all still show clear caustic shell structure. It is at the edge of these shells where the breaks in the profiles occur. These few contributors determine the overall profile and, at some radii, almost the entire stellar mass comes from a single progenitor. For example, around 50 kpc the overall density profile is almost entirely determined by the 2nd largest contributor. It is clear that the break in the overall profile is due to this object.

It can be argued that when measuring the spherically averaged stellar halo density profile, coherent structures such as those just described should be removed. However, while a massive stream such as the Sagittarius stream in the Milky Way might be easy to exclude, objects in later stages of disruption are more difficult to identify. In the simulations we are able to use the SUBFIND halo finder to identify bound structures and follow the accretion histories of stars in order to find candidate streams but, unfortunately, this cannot be done with observational data. In addition, even if structures have been identified, the question is then how to decide whether they should be excluded from the halo. For these reasons, as the overall profile is so sensitive to individual accretion events, and thus is likely to change rapidly with time, it is not clear how useful it is to measure the

density profile of a stellar halo, other than for the purpose of gaining information about recent large accretion events.

As has been seen in Fig. 5, the spherically averaged density profile is not sensitive to the type of tracer used and this suggests that observations based on any type of tracer will reliably recover the profile in a given region of the sky. What is much more important is the area of the sky over which the profile is measured. In order to measure the profile to large radii, narrow pencil-beam surveys are often used. Such surveys can probe deep into the stellar halo, but have limited area. In order to quantify the intrinsic differences in the slope of the profile in different directions we can employ a similar observational strategy as Sesar et al. (2011) and measure the profiles of the stellar haloes in the simulations in limited size patches. Sesar et al. (2011) used four pencil-beams from the CFHTLS to select near-MSTO stars and measure the slope of the halo between 5 and 35 kpc.

We can select the same types of stars as Sesar et al. (2011) and measure the profile in  $8 \times 8$  degree<sup>2</sup> patches. However, we are not limited to testing just four directions, but we can measure the profile in many directions evenly spaced over the whole sky. We focus on just the slope of the profile in the 5 to 35 kpc range. These results can then be directly compared to the true profiles and provide a test of how well previous pencil-beam surveys have recovered the actual profile of the Milky Way. Fig. 7 shows an all-sky map colour-coded by the slope of the density profile in Aq-A. For each pencil beam we have found the parameters of the best-fit power law,  $\rho \propto r^n$ . It can be immediately seen that there is a massive variation in slope over the sky, ranging very steep,  $n = -5$ , profiles in some areas, to flat,  $n = 0$ , profiles in others.

At the very centre of the map is the Galactic Centre, where the slope is steepest and the profile is smoothest. In the opposite direction, at the edges of the map (looking towards the Galactic anti-Centre) there is much greater variation, with many patches exhibiting very flat slopes. These areas with flat slopes can be associated with directions that go through substructure. It seems that in Aq-A the greatest abundance of structure lies in the Galactic Plane, just outside of the Solar Circle. This is also true, to a lesser extent, of several of the other haloes. Only when looking near the Galactic North and South pole could the stellar halo be described as being anything like smooth.

In order to quantify just how much the slope varies over the sky, the distributions of the pencil-beam slopes are shown in Fig. 8 for all five haloes. On each of these, a vertical dashed line marks the value measured for the overall slope from the spherically averaged density profile. For Aq-A, B and C the overall slope is relatively close to either the median or the peak of the distribution, but for Aq-D and E the overall slope is significantly different, lying at the steep end of the distribution. This can be explained by the fact that, as we saw earlier, a single substructure limited to a very small spatial region can completely dominate the overall profile, radically changing it from the profile that would be measured in any other part of the halo.

It should be noted that we have been examining the slope of the profile between 5 to 35 kpc region. In the Milky Way, in the inner part of this region ( $r < 20$  kpc) the in-situ component of the stellar halo is likely to be important, and also likely to be much smoother than the accreted halo

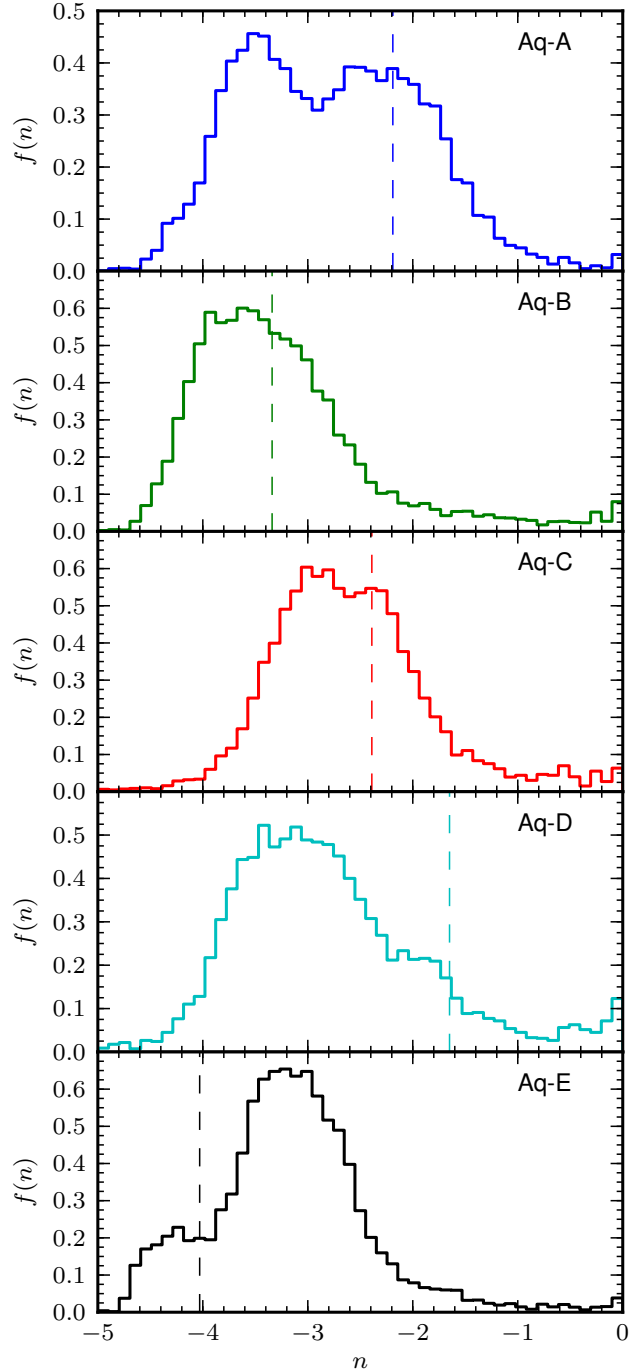


**Figure 8.** The distribution of the slopes of the density profile measured using pencil-beam samples of stars across the sky. The dashed vertical lines mark the overall slope as measured from the spherically averaged density profile.

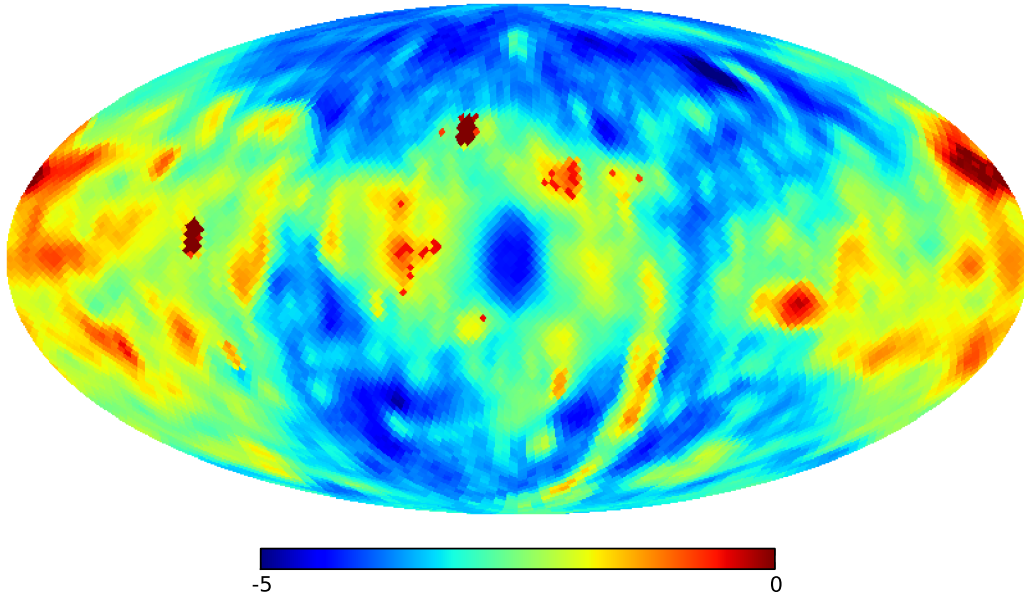


**Figure 7.** An all sky map showing the slope of the stellar density profile between 5 and 35 kpc in different directions measured using pencil beams. The Galactic Centre is at the centre of the map and the disc plane is oriented horizontally. A total of 12,288 8x8 degree beams were used, equally spaced over the sky. The colours indicate the best-fit power-law slope in each direction.

component constructed from disrupted satellites. This could reduce the variation in the density profile, but the presence of any substructure is still likely to dominate and skew any attempts to measure the overall stellar halo density profile.

## 5 TRACER DISTRIBUTION OVER THE SKY

In the previous section we showed that the distributions of different kinds of stellar tracers in our mock catalogues are not noticeably different when averaged over global scales. In this section we examine whether local variations amongst the different tracers exist. It has been proposed that localized variations in the mix of stellar populations may provide a method for discovering new, previously unknown structures in the Milky Way halo. Such signatures have already been found in known structures. For example, significant fluctuations in the ratio of BHB to MSTO stars have been found in the stellar halo (Bell et al. 2010). Some structures, such as the “low-latitude stream” are almost devoid of BHBs, while other structures are rich in them. The Sagittarius tidal stream even shows a variation in the BHB/MSTO ratio along its extent, which has been interpreted as arising from a population gradient in the progenitor dwarf galaxy. In this section we perform a similar test with the BHB, MSTO and K giant samples from our mock catalogues and attempt to understand the origin of the differences.

The simplest way to achieve this is to search for variations by comparing all-sky maps of the projected number density for our different tracers as seen by a hypothetical observer located on the solar circle. Fig. 9 shows a number of such maps for the Aq-C halo. We focus on the Aq-C halo as it contains several interesting and noteworthy features.

It contains many clearly defined streams that are visible in all the tracers. What is most interesting, however, is that there are two streams that do not appear in the BHB map but appear in the two other maps. In particular, the large continuous horizontal stream lying close to the equatorial plane that can be clearly seen in the MSTO and K giant map is partially missing in the BHB map, while the shorter stream located near the top of the MSTO map, towards the galactic north pole, is totally absent in the BHB map.

By looking at the ratio of the different tracers over the sky, it is very easy to see exactly where the differences in the composition of the stellar populations occur. Comparing the ratio of BHBs/MSTO stars the two missing streams are easily identifiable. While the large, equatorial stream is at least partially present in the BHB map, it has a lower than average abundance resulting in a slightly higher MSTO/BHB ratio. In contrast, the stream near the top of the MSTO map is completely absent in the BHB map and has a huge MSTO/BHB ratio. Other streams with more standard stellar populations have BHB to MSTO stars ratios similar to that of the overall halo and thus do not show up in the ratio maps. There are also differences in the MSTO/K giant ratio, but in the opposite sense. From the MSTO/K giant map it can be seen that the two streams have a higher than average abundance of K giants. One other feature is that the BHB stars have a slightly higher than average abundance in the galactic centre.

All these differences in the relative abundance of the three types of tracer can be explained by differences in the age and metallicity of the stellar populations that make up these features. In Fig. 10 we show a map of the average age (left) and the average metallicity (right) of the Aq-C stellar halo. These have been generated from the mean

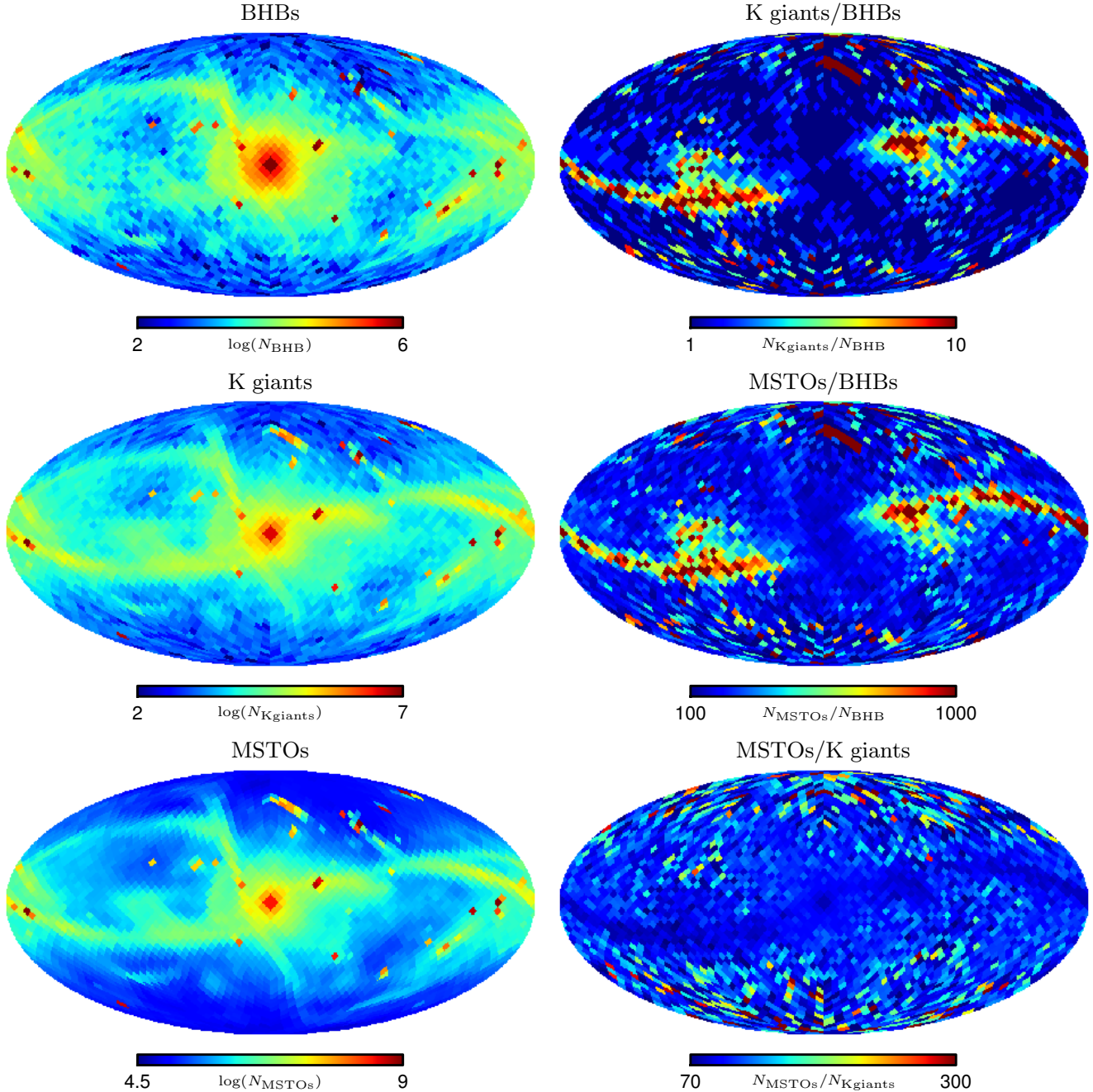


**Figure 9.** The distribution of different stellar tracers over the sky for the Aq-C stellar halo as “seen” by a hypothetical observer located on the solar circle. The Galactic Centre is at the centre of the map and the disc plane is oriented horizontally. *Left column:* the projected logarithmic number density of BHBs, K giants and MSTO stars. *Right column:* the ratio of K giants/BHBs, MSTO/BHBs and MSTO/K giant stars.

age/metallicity of all stars within each equally sized bin on the sky. It is immediately obvious that the streams missing from the BHB map are composed of the very youngest stars in the halo and, as well as being a few gigayears younger than the mean, they are also slightly more metal rich. In these populations BHB stars have not yet had time to form, which explains their deficit. The actual age of these structures may be even younger, but the average is increased by the other non-associated halo stars along the same line-of-sight. Interestingly, there is a patch of intermediate age

stars that stands out in the lower right hand corner of the age map, but is not visible in any of the tracer maps. This suggests that while differences in the make up of stellar populations will help identify some structures, not all will be found with this technique.

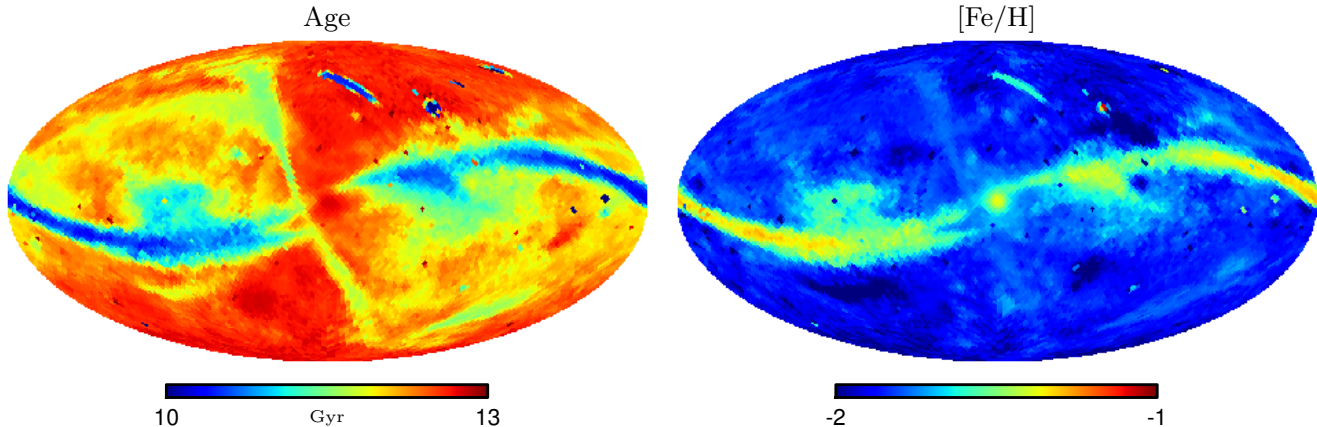


**Figure 10.** All-sky maps of the mean properties of the Aq-C stellar halo when averaged along the line of sight. *Left map:* average age. *Right map:* average metallicity map.

## 6 CONCLUSIONS

In this paper we have described a new way to construct mock catalogues of stellar haloes based on cosmological  $N$ -body simulations. We have adopted the particle tagging method of Cooper et al. (2010) and extended it to turn the output into a catalogue of individual stars that can be directly compared to observations.

Using the Aquarius  $N$ -body simulations of galactic haloes as the basic framework, we employed the semi-analytical galaxy formation model, GALFORM, to calculate the evolution of the baryonic component of the Universe. This predicts the amount and properties of the stellar material forming in each halo throughout the simulation. These stellar populations were used to tag dark matter particles in the simulation. Finally, these tags are turned into a mock catalogue using theoretical isochrones to convert the fundamental properties of the stellar populations, such as age and metallicities, into a set of observables such as colour and magnitudes. A phase-space sampling technique was then applied to “explode” the massive particles into numerous individual stars while maintaining the phase-space structure of the original simulation.

The output of our method represents a perfect dataset containing precise information about the entire galaxy. Actual observations usually provide an incomplete, limited view of a galaxy. They may be subject to selection criteria, be limited in coverage, or, in the case of surveys of the stellar halo, be obstructed by other structures such as the galactic disc. To make a fair comparison between simulations and observations, it is necessary to convert the simulation data into a form that shares the same limitations and biases as the observational data. The selection criteria of an actual survey, encoded in a mask or selection function, can be readily applied to our mocks, and observational errors can also be easily modeled. Thus, in principle, the mock catalogues could be viewed and analyzed in an identical manner to observational data. In this paper, we have used the Aquarius simulations to make mock catalogues of galactic stellar haloes that can be used to help interpret data from upcoming surveys such as those to be carried out by the GAIA mission. However, there is no reason why this technique could

not be applied to other simulations of both smaller haloes, such as dwarfs, or larger haloes, such as clusters.

Using our mock catalogues we carried out simple analyses to explore whether current observations of the Milky Way halo provide an accurate picture. We have found that:

- The accreted stellar halo is mainly built up from a few massive objects. Those that are in early stages of disruption still maintain a coherent structure and are locally concentrated. They dominate the spherically averaged density profile at their corresponding radii. Since the overall density profile is so sensitive to these few substructures it provides limited information about the structure of the underlying dark matter halo. Instead, it tells us about the recent accretion history. Three of the five haloes we have investigated show clear breaks in their spherically averaged density profiles while two are well described by a single power-law. These breaks have nothing to do with the distinction between accreted and in-situ components as has often been claimed for the Milky Way halo nor with the recent accretion of a satellite (Deason et al. 2013).
- The structure of the accreted stellar halo is clumpy and thus varies considerably over the sky. Attempts to measure properties of the halo, such as its density profile, based on limited regions of the sky provide biased estimates. For example, if the profile is modeled as a single power-law, the slopes measured in different pencil-beam surveys through our mock stellar haloes vary from very steep to flat depending on the direction of the survey.
- Difference in the ages and metallicities of the satellites that build up the stellar halo induce local variations in the composition of the stellar populations. These are reflected in differences in the abundance of different stellar types. For example young, more metal rich objects tend to lack BHB stars. Searching for such differences offers a way to identify streams and structure in the halo.

In this paper we have applied the method of converting massive stellar particles into stars to the output of the tagging method of Cooper et al. (2010) applied to  $N$ -body simulations. However, with only very little modification it should be possible to use the same conversion technique on hydrodynamical galaxy formation simulations. In this way, components that are missing from our treatment, such as

the galactic disk or bulge, could be included while components, such as the stellar halo, could be followed with much higher resolution than is attainable with current hydrodynamic simulations.

The five complete mock catalogues for the Aquarius haloes A-E, will be made publicly available at <http://virgodb.dur.ac.uk:8080/MyMillennium>, in a database that can be queried via SQL. The properties that are available in each catalogue are described in the Table 1.

## ACKNOWLEDGMENTS

This work was supported by the European Research Council [grant number GA 267291] COSMIWAY and Science and Technology Facilities Council [grant number ST/F001166/1,ST/L00075X/1]. APC acknowledges a Chinese Academy of Sciences International Research Fellowship and NSFC grant no. 11350110323. The simulations for the Aquarius Project were carried out at the Leibniz Computing Centre, Garching, Germany, at the Computing Centre of the Max-Planck-Society in Garching, at the Institute for Computational Cosmology in Durham, and on the STELLA supercomputer of the LOFAR experiment at the University of Groningen.

## REFERENCES

- Akhter S., Da Costa G. S., Keller S. C., Schmidt B. P., 2012, *ApJ*, 756, 23
- Arad I., Dekel A., Klypin A., 2004, *MNRAS*, 353, 15
- Baugh C. M., 2006, *Reports on Progress in Physics*, 69, 3101
- Bell E. F., Xue X. X., Rix H.-W., Ruhland C., Hogg D. W., 2010, *AJ*, 140, 1850
- Bower R. G., Benson A. J., Malbon R., Helly J. C., Frenk C. S., Baugh C. M., Cole S., Lacey C. G., 2006, *MNRAS*, 370, 645
- Bressan A., Marigo P., Girardi L., Salasnich B., Dal Cero C., Rubele S., Nanni A., 2012, *MNRAS*, 427, 127
- Bullock J. S., Johnston K. V., 2005, *ApJ*, 635, 931
- Carollo D., et al., 2007, *Nature*, 450, 1020
- Carollo D., et al., 2010, *ApJ*, 712, 692
- Cole S., Lacey C. G., Baugh C. M., Frenk C. S., 2000, *MNRAS*, 319, 168
- Colless M., et al., 2001, *MNRAS*, 328, 1039
- Cooper A. P., et al., 2010, *MNRAS*, 406, 744
- Crain R. A., et al., 2009, *MNRAS*, 399, 1773
- de Bruijne J. H. J., 2012, *Ap&SS*, 341, 31
- De Propris R., Harrison C. D., Mares P. J., 2010, *ApJ*, 719, 1582
- Deason A. J., Belokurov V., Evans N. W., 2011, *MNRAS*, 416, 2903
- Deason A. J., Belokurov V., Evans N. W., Johnston K. V., 2013, *ApJ*, 763, 113
- D’Onghia E., Springel V., Hernquist L., Keres D., 2010, *ApJ*, 709, 1138
- Font A. S., McCarthy I. G., Crain R. A., Theuns T., Schaye J., Wiersma R. P. C., Dalla Vecchia C., 2011a, *MNRAS*, 416, 2802
- Font A. S., et al., 2011b, *MNRAS*, 417, 1260
- Gao L., Navarro J. F., Cole S., Frenk C. S., White S. D. M., Springel V., Jenkins A., Neto A. F., 2008, *MNRAS*, 387, 536
- Helmi A., 2008, *A&ARv*, 15, 145
- Jordi C., Gebran M., Carrasco J. M., de Bruijne J., Voss H., Fabricius C., Knude J., Vallenari A., Kohley R., Mora A., 2010, *A&A*, 523, A48
- Kaiser N., et al., 2010, *SPIE*, 7733
- Kazantzidis S., Kravtsov A. V., Zentner A. R., Allgood B., Nagai D., Moore B., 2004, *ApJ*, 611, L73
- Keller S. C., Murphy S., Prior S., Da Costa G., Schmidt B., 2008, *ApJ*, 678, 851
- Kennicutt Jr. R. C., 1983, *ApJ*, 272, 54
- Lewis G. F., et al., 2013, *ApJ*, 763, 4
- Prusti T., 2012, *AN*, 333, 453
- Morrison H. L., Flynn C., Freeman K. C., 1990, *AJ*, 100, 1191
- Morrison H. L., Mateo M., Olszewski E. W., Harding P., Dohm-Palmer R. C., Freeman K. C., Norris J. E., Morita M., 2000, *AJ*, 119, 2254
- Navarro J. F., et al., 2010, *MNRAS*, 402, 21
- Pasetto S., Chiosi C., Kawata D., 2012, *A&A*, 545, A14
- Sawala T., Frenk C. S., Crain R. A., Jenkins A., Schaye J., Theuns T., Zavala J., 2013, *MNRAS*, 431, 1366
- Schönrich R., Binney J., Dehnen W., 2010, *MNRAS*, 403, 1829
- Sesar B., et al., 2010, *ApJ*, 708, 717
- Sesar B., Jurić M., Ivezić Ž., 2011, *ApJ*, 731, 4
- Sharma S., Bland-Hawthorn J., Johnston K. V., Binney J., 2011, *ApJ*, 730, 3
- Sharma S., Steinmetz M., 2006, *MNRAS*, 373, 1293
- Spergel D. N., et al., 2003, *ApJS*, 148, 175
- Springel V., et al., 2008a, *MNRAS*, 391, 1685
- Springel V., et al., 2008b, *Nature*, 456, 73
- Starkenburger E., et al., 2009, *ApJ*, 698, 567
- Tissera P. B., White S. D. M., Scannapieco C., 2012, *MNRAS*, 420, 255
- Vogelsberger M., et al., 2014, *Natur*, 509, 177
- Watkins L. L., et al., 2009, *MNRAS*, 398, 1757
- Xue X.-X., et al., 2012, *ArXiv e-prints*
- Yanny B., et al., 2009, *AJ*, 137, 4377
- York D. G., et al., 2000, *AJ*, 120, 1579
- Zolotov A., Willman B., Brooks A. M., Governato F., Hogg D. W., Shen S., Wadsley J., 2010, *ApJ*, 721, 738